Shape-Controlled Synthesis of Colloidal Superparticles from Nanocubes

Tie Wang,[†] Xirui Wang,[†] Derek LaMontagne,[†] Zhongliang Wang,[†] Zhongwu Wang,[‡] and Y. Charles Cao*,[†]

[†]Department of Chemistry, University of Florida, Gainesville, Florida 32611, United States
[‡]Cornell High Energy Synchrotron Source, Wilson Laboratory, Cornell University, Ithaca, New York 14853, United States

Ⓢ Supporting Information

ABSTRACT: This communication reports a shape-controlled synthesis of colloidal superparticles (SPs) from iron oxide nanocubes. Our results show that the formation of SPs is under thermodynamic control and that their shape is determined by Gibbs free energy minimization. The resulting SPs adopt a simple-cubic superlattice structure, and their shape can be tuned between spheres and cubes by varying the relative free energy contributions from the surface and bulk free energy terms. The formation of sphere-shaped SPs from nanocubes suggests that the size-dependent hydration effect predicted by the Lum−Chandler−Weeks theory plays a very important role in the self-assembly of nano-objects. In addition, the iron oxide SPs exhibit shape-dependent therapeutic effects in magnetomechanical treatments of cancer cells in vitro.

Colloidal superparticles (SPs) are nanoparticle assemblies in the form of colloidal particles.[1] These SPs—a new class of building blocks for making functional materials—exhibit chemical and physical properties inherited from their constituent nanoparticles as well as collective properties induced by the electronic, plasmonic, and/or magnetic coupling between their constituents.[1,2] Because of their colloidal form, SPs are solution-processable and thus can be cost-effectively assembled into designed meso-/macrostructures for use in applications such as solar cells, light-emitting diodes, and solid-state catalysts.[3] In general, the nanoparticle packing order in SPs can be either short-range (i.e., amorphous) or long-range (i.e., supercrystalline),[1,2d,3c,4] and the long-range translational order in the nanoparticle packing enables supercrystalline SPs to exhibit more defined collective properties because these properties are largely dependent on the interparticle spacing and packing configuration of the constituent nanoparticles in the SPs.[5] To date, several approaches for synthesizing colloidal SPs from constituent nanoparticles with uniform or nonuniform size distributions have been developed, but most are able to make only spherical SPs.[1,2d,3c,4] Less is known about shape control in the synthesis of colloidal SPs.

Here we report the shape-controlled synthesis of supercrystalline SPs with a cubic or spherical shape from identical constituents, namely, iron oxide nanocubes. Our results show that although their shapes are different, these two types of colloidal SPs adopt the same simple-cubic superlattice, and

both of them can be effectively uptaken by cultured LNCaP human prostate cancer cells. Upon exposure to a low-frequency pulsed magnetic field (4 Hz), the SPs displayed shape-dependent destruction of cultured LNCaP cancer cells, with the cube-shaped SPs leading to a higher cancer-cell destruction rate ($89.0 \pm 6.5\%$) than the spherical SPs ($54.0 \pm 2.1\%$).

The shape-controlled SP synthesis was designed on the basis of a previously developed approach in which SPs are formed through controlled induction of solvophobic interactions (CIS).[1a,b] The CIS approach utilizes water-soluble nanocrystal micelles as precursors. Upon the introduction of the nanocrystal micelles into a solvent such as ethylene glycol, the hydrophobic van der Waals interactions between the hydrocarbon chains of the nanocrystal ligands (e.g., oleic acid on Fe_3O_4 nanocrystals) and the hydrocarbon chains of the micelle surfactant (e.g., dodecyltrimethylammonium bromide, DTAB) are weakened, thus leading to decomposition of the nanoparticle micelles and the subsequent formation of SPs mediated by the solvophobic interactions between the nanoparticle surface and the solvent molecules (Scheme 1). Our previous results showed that the size of SPs is controlled by a kinetic growth process, whereas their shape is under thermodynamic control.[1a,b]
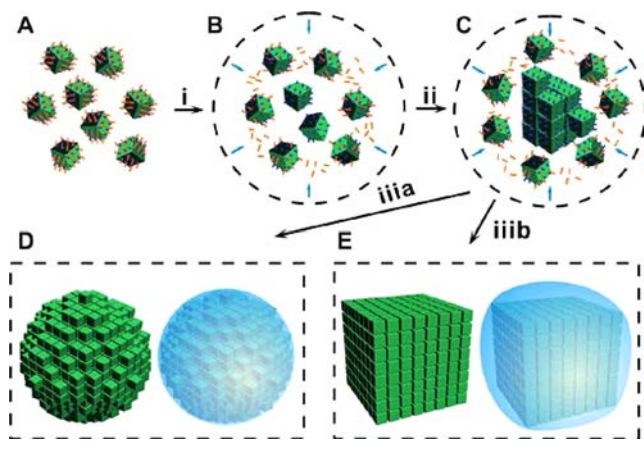
Under thermodynamic control, a colloidal SP—like a crystal formed from atomic or molecular building blocks—adopts an equilibrium structure as predicted by the Wulff construction,[6] wherein the SP exhibits a minimized Gibbs free energy (G): $G = G_b + S\gamma$, where G_b is the bulk Gibbs free energy and S and γ are the surface area and surface tension of the SP, respectively. The γ value, which is positive, is determined by the repulsive solvophobic interactions between the SP and the surrounding water and ethylene glycol molecules.[7] G_b, which is negative, is determined by interparticle interactions between neighboring nanocrystals, including van der Waals interactions between their inorganic cores as well as between their surface ligands.[8] A larger total interaction energy within an SP is associated with a more negative value of G_b. When the constituent nanocrystals are spheres, the resulting SPs adopt a close-packed superlattice structure to minimize the bulk free energy and a spherical shape to minimize the surface free energy.[1a,b] On the contrary, when the constituent nanocrystals are nanocubes, a superlattice having a simple-cubic structure is often associated with the

Scheme 1. Formation of Colloidal SPs from Iron Oxide Nanocubes: (A) Nanocube Micelles; (B, C) SP Embryo; (D) Spherical and (E) Cube-Shaped SPs; (i) Embryo Formation, (ii) Nanocube Crystallization, and (iii) SP Formation

and then evaporating the chloroform by bubbling of Ar to at 40 °C. Next, under vigorous stirring, the nanocube micelle solution was injected into a three-neck flask with an ethylene glycol solution of polyvinylpyrrolidone (PVP) (2.0 mM, 5.0 mL). After the mixture was stirred for 10 min, the resulting SPs were purified by centrifugation and redispersed in polar solvents (e.g., water and ethanol) at a variety of concentrations.

Low-magnification transmission electron microscopy (TEM) images showed that these SPs were spheres having a diameter of 260 nm with an RSD of 14% (Figure 1A). Higher-
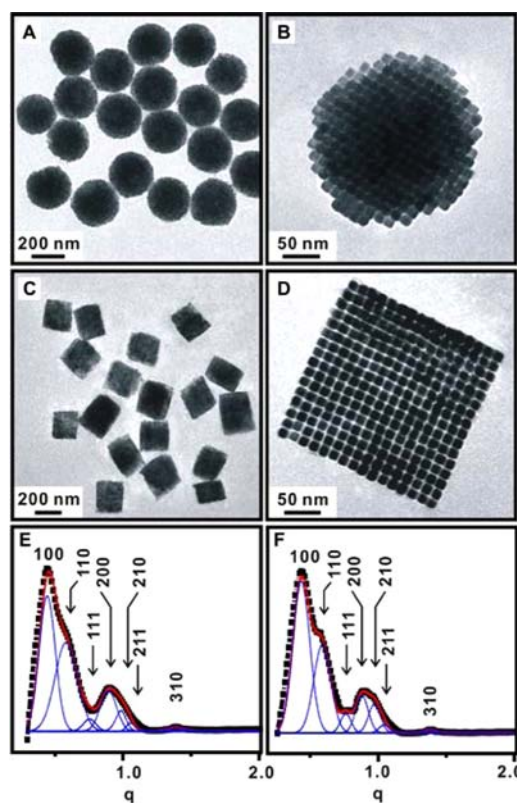

Figure 1. (A−D) TEM images of (A) sphere-shaped SPs, (B) a spherical SP viewed along the [001] zone axis, (C) cube-shaped SPs, and (D) a cubic SP viewed along the [001] zone axis. (E, F) SAXS patterns of (E) spherical and (F) cube-shaped SPs. Fitted peaks are shown in blue.[9]

minimized bulk free energy: $G_b = NE_p$, where N is the total number of closest nanocube contacts in an SP and E_p, a negative number, is the interaction energy between two neighboring nanocubes. However, it is unclear which equilibrium shape is adopted by the SP.

In principle, a perfect spherical SP formed from nanocubes should possess a surface consisting of kinks and steps (Scheme 1D, left) and have a surface area of $S \approx 6\pi R^2$, where R is the SP radius (see Figure S1 in the Supporting Information).[9] This surface area would be larger than that of a cube-shaped SP made of an identical number of nanocubes (Scheme 1E, left), and thus, a spherical SP should have a larger surface free energy than a cube-shaped SP. In addition, because it has more constituent nanocubes on the surface, the spherical SP should have a smaller N and hence a less negative G_b than its cubic counterpart. Therefore, the cube-shaped SPs should have a lower Gibbs free energy than the spherical SPs, and their formation should be favored thermodynamically. However, according to the Lum−Chandler−Weeks (LCW) theory,[10] solvent molecules (i.e., water and ethylene glycol in this study) cannot effectively wet all of the concave areas on the spherical SP surface when the length scale of these kinks and steps is less than 100 nm. Therefore, when the size of its constituent nanocubes is small (e.g., <50 nm), the "effective surface area" of the SP would decrease to a value close to $4\pi R^2$ (Scheme 1D, right), thus leading to a smaller surface energy than for the cube-shaped SP (Scheme 1E, right). As a result, the equilibrium shape of SPs is determined by the interplay between the bulk and surface free energy terms in minimizing the overall Gibbs free energy. Thus, the shape of SPs can be tuned between spheres or cubes by varying the values of E_p and γ.

To examine whether the wettability (or size dependent hydration) predicted by the LCW theory plays a role in the formation of SPs, we used iron oxide nanocubes [edge length = 11.0 nm with a relative standard deviation (RSD) of 4.8%] as constituents to synthesize colloidal SPs (Figure S2). Thermogravimetric analysis results (Figure S3) showed that these iron oxide nanocubes have 1500 oleate ligands per particle (~40% surface coverage).[9] In a typical SP synthesis, a clear aqueous solution of nanocube micelles was prepared by mixing a chloroform solution of iron oxide nanocubes (28 μM, 1 mL) with an aqueous solution of DTAB (65.0 μmol, 1 mL)

magnification images from tilting experiments (Figure 1B) revealed that the SPs were composed of iron oxide nanocubes packed in a simple-cubic lattice that could be indexed as the [100] zone projection of a simple-cubic superlattice with a lattice constant of 14.0 nm. These SPs could also display a two-dimensional lamellar striped pattern associated with the projections of the [0kl] zones of this simple-cubic superlattice (Figure 2B,C).[11] The superlattice structure was further confirmed by synchrotron-based small-angle X-ray scattering (SAXS). A typical SAXS pattern of these SPs consisted of a group of peaks that could be indexed as the (100), (110), (111), (200), (210), (211), and (310) Bragg diffraction peaks of a simple-cubic lattice with a lattice constant of 14.0 ± 0.2 nm (Figure 1E,F). Collectively, these data further demonstrated that the interparticle distance in the superlattices was 3.0 nm, indicating that oleate ligands were partially intercalated into the gaps between neighboring nanocubes.[12]
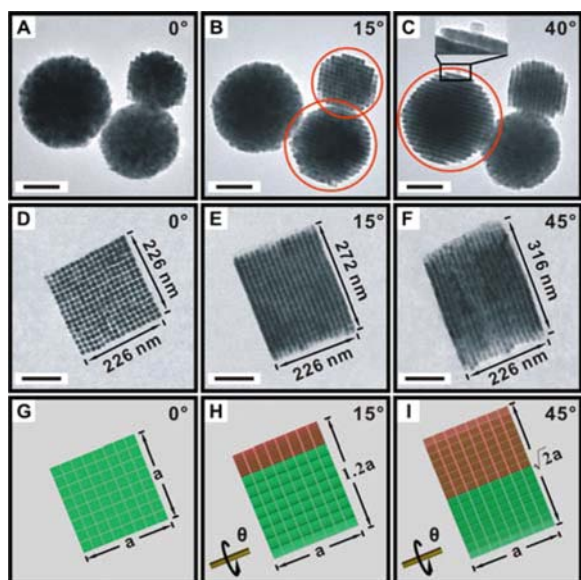
Figure 2. (A–F) TEM images of (A–C) spherical and (D–F) cube-shaped SPs at the tilting angle indicated in each panel. The inset in (C) shows a zoomed-in image of the "north pole" part of the SP. (G–I) Schematic illustrations of a cubic SP model at the tilting angle indicated in each panel. The scale bars are 100 nm.

The formation of spherical SPs is consistent with the prediction of the LCW theory under conditions where the surface free energy term dominates over the bulk free energy term in the minimization of the SP Gibbs free energy. These condition are in agreement with the existence of adparticles—nanoscopic counterparts of adatoms in crystal formation—that lie on the poles of the spherical SPs (Figure 2C inset);[13] this packing configuration is extremely unfavored in the minimization of the bulk free energy of the SP.[14] In addition, if SP formation from nanocubes is affected by the wettability predicted the LCW theory, one should be able to make cube-shaped SPs by increasing the interparticle interaction energy (i.e., the absolute value of E_p) and/or decreasing the value of γ for the SPs.

To explore this possibility, we modified the typical SP synthesis by introducing a small amount of oleic acid (0.04 mL) into the SP growth solution. Using iron oxide nanocube constituents from the same batch as the ones used for making spherical SPs, we indeed obtained cube-shaped SPs having an edge length of 209 nm with an RSD of 18% (Figure 1C); their average volume was nearly identical to that of the spherical SPs obtained from the synthesis without additional oleic acid. TEM observations and SAXS measurements consistently revealed that the cube-shaped SPs displayed a simple-cubic superlattice with a lattice constant of 14.1 ± 0.2 nm (Figure 1D), nearly identical to that of their spherical counterparts (14.0 ± 0.2 nm). The cubic shape of the SPs was unambiguously distinguished from square plates by the results of TEM tilting experiments (Figure 2D–F): (1) square-shaped SP images appeared only with the [100] zone projection of the simple-cubic superlattice; (2) the rectangle-shaped images were always associated with a lamellar striped pattern; and (3) the rectangle width (a) did not change as the tilt angle (θ) was varied, whereas the length (l) varied as a function of θ according to $l = a(\sin\theta + \cos\theta)$ (Figure 2G–I).

The formation of cube-shaped SPs further confirmed that the wettability predicted by LCW theory plays a major role in the formation of SPs from hydrophobic nanocubes. In principle, the addition of oleic acid into the SP growth solution should increase the number of oleate ligands on iron oxide nanocubes, which in turn should increase the interparticle interactions originating from the van der Waals interactions due to the intercalation of hydrocarbon chains.[4b,15] In addition, because γ of the SPs is determined by interactions among the oleate ligands on the iron oxide nanocubes, DTAB, and molecules of the medium (water and ethylene glycol), the existence of free oleic acid in the SP growth solution should decrease γ because of the interactions between the positively charged DTA group and the negatively charged oleate group. Indeed, when a larger amount of oleic acid (0.10 mL) was added into the SP growth solution, the synthesis yielded only aggregated SPs (Figure S4); this result is associated with a small surface tension and decreased electrostatic double-layer interactions between SPs.

Moreover, the data from superconducting quantum interference device (SQUID) measurements (Figure S5) indicated that the resulting spherical and cube-shaped SPs were superparamagnetic. They had nearly identical average volumes and consisted of ~4000 iron oxide nanocubes. Therefore, these SPs could exhibit a large net magnetic moment under an external magnetic field, allowing them to be used as the principal agents to achieve magnetomechanical cancer therapy.[16] In this therapy, magnetic particles—manipulated by an external magnetic field—generate mechanical forces on the cellular organelles of targeted cells, leading to cell destruction and death.[16] We used the LNCaP human prostate cancer cells as a model system to evaluate the efficacy of SP-based magnetomechanical therapy. In a typical experiment, the LNCaP cells were respectively incubated with the spherical and cube-shaped SPs for 12 h and then washed thoroughly with fresh culture medium (notably, an inductively coupled plasma mass spectrometry assay showed that the spherical and cube-shaped SPs exhibited nearly identical rates of internalization into the LNCaP cells: ~270 SPs per cell).[9] Afterward, the cells were exposed to a 4 Hz pulsed magnetic field (pulse length = 4.0 ms; field gradient ΔB = 6.48 kG/cm) for 10 min (Figure 3A), and then the cells were further cultured under standard conditions for 2 h. The cell viability was semiquantitatively evaluated using a two-dye LIVE/DEAD cell viability assay (Invitrogen, Carlsbad, CA). Fluorescence microscopy showed that the pulsed magnetic field did not cause measurable death of the cells without SPs (Figure 3B) but induced a significant amount of death of LNCaP cells containing either the spherical or cube-shaped SPs (Figure 3C,D), with the latter inducing more pronounced cell death than the former (Figure 3C,D). In contrast, SP-containing cells that were not exposed to the magnetic field showed no measurable cell death (Figure S6), further indicating that the pulsed magnetic field exposure was essential for SP-induced cell destruction.

These results were further confirmed by the results from a quantitative CellTiter-blue cell viability assay (Promega, San Luis Obispo, CA), which showed that magnetomechanical treatments with the spherical SPs decreased the cell viability by 54.0 ± 2.1%, whereas an 89.0 ± 6.5% decrease in cell viability was caused by the treatments with cube-shaped SPs (Figure 3E). In our experiments, the magnetic-field-induced forces applied onto cell organelles by the spherical and cube-shaped SPs were nearly identical and could be calculated as 129 ± 41 fN.[9] The therapeutic effects of the magnetomechanical treatments are due in part to the perturbations of cellular membrane integrity and the membrane integrity of cellular
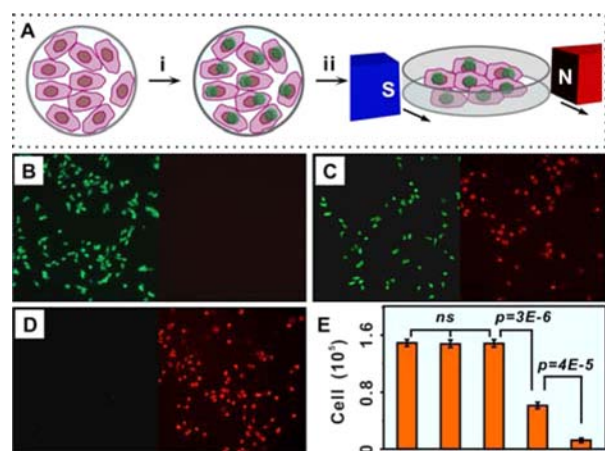
Figure 3. (A) Schematic illustration of magnetomechanical cancer-cell destruction: (i) SP endocytosis into cultured LNCaP cells; (ii) exposure of the cells to a pulsed magnetic field created by rotating permanent magnets. (B−D) Fluorescence imaging analyses of the LIVE/DEAD cell viability assays of the magnetic-field-exposed LNCaP cells (B) without SPs as the blank control, (C) containing spherical SPs, and (D) containing cube-shaped SPs. The green channel monitors live cells and the red channel monitors dead cells. (E) Data from the CellTiter-blue cell viability assay of magnetic-field-exposed LNCaP cells (1) without SPs, (4) with spherical SPs, and (5) with cube-shaped SPs and LNCaP cells not exposed to the magnetic field with (2) spherical and (3) cube-shaped SPs. The p values were determined from the results of five parallel experiments, where nonsignificance (ns) is indicated by $p > 0.32$.

organelles (e.g., endosomes).[16a,17] The shape-dependent therapeutic effects can be attributed to (1) large effective pressures induced by the sharp corners and edges of the cube-shaped SPs (Figure S7) and (2) wettability differences between the spherical and cube-shaped SPs (Figure S8).

In summary, we have demonstrated a shape-controlled synthesis of SPs from iron oxide nanocubes. The resulting SPs adopt a simple-cubic superlattice structure and exhibit either a spherical or cubic shape in a controllable manner. The formation of sphere-shaped SPs reveals that the size dependence of hydration predicted by the LCW theory plays a significant role in the self-assembly of nano-objects. In addition, the resulting iron oxide SPs display shape-dependent therapeutic effects in magnetomechanical treatments of cancer cells in vitro. These findings may shed new light on the synthesis of size- and shape-controlled nanocrystal assemblies as well as their use in biomedical applications.

ASSOCIATED CONTENT

S Supporting Information

Experimental details and additional data. This material is available free of charge via the Internet at http://pubs.acs.org.

AUTHOR INFORMATION

Corresponding Author
cao@chem.ufl.edu

Notes
The authors declare no competing financial interest.

ACKNOWLEDGMENTS

REFERENCES

(1) (a) Zhuang, J. Q.; Wu, H. M.; Yang, Y. A.; Cao, Y. C. *J. Am. Chem. Soc.* **2007**, *129*, 14166. (b) Zhuang, J. Q.; Wu, H. M.; Yang, Y. G.; Cao, Y. C. *Angew. Chem., Int. Ed.* **2008**, *47*, 2208. (c) Xia, Y. S.; Nguyen, T. D.; Yang, M.; Lee, B.; Santos, A.; Podsiadlo, P.; Tang, Z. Y.; Glotzer, S. C.; Kotov, N. A. *Nat. Nanotechnol.* **2011**, *6*, 580. (d) Lu, Z. D.; Yin, Y. D. *Chem. Soc. Rev.* **2012**, *41*, 6874.

(2) (a) Beverly, K. C.; Sample, J. L.; Sampaio, J. F.; Remacle, F.; Heath, J. R.; Levine, R. D. *Proc. Natl. Acad. Sci. U.S.A.* **2002**, *99*, 6456. (b) Choi, C. L.; Alivisatos, A. P. *Annu. Rev. Phys. Chem.* **2010**, *61*, 369. (c) Murray, C. B.; Kagan, C. R.; Bawendi, M. G. *Annu. Rev. Mater. Sci.* **2000**, *30*, 545. (d) Bai, F.; Wang, D. S.; Huo, Z. Y.; Chen, W.; Liu, L. P.; Liang, X.; Chen, C.; Wang, X.; Peng, Q.; Li, Y. D. *Angew. Chem., Int. Ed.* **2007**, *46*, 6650.

(3) (a) Yamada, Y.; Tsung, C. K.; Huang, W.; Huo, Z. Y.; Habas, S. E.; Soejima, T.; Aliaga, C. E.; Somorjai, G. A.; Yang, P. D. *Nat. Chem.* **2011**, *3*, 372. (b) Zhuang, J. Q.; Shaller, A. D.; Lynch, J.; Wu, H. M.; Chen, O.; Li, A. D. Q.; Cao, Y. C. *J. Am. Chem. Soc.* **2009**, *131*, 6084. (c) Klajn, R.; Bishop, K. J. M.; Fialkowski, M.; Paszewski, M.; Campbell, C. J.; Gray, T. P.; Grzybowski, B. A. *Science* **2007**, *316*, 261. (d) Lu, Z. D.; Ye, M. M.; Li, N.; Zhong, W. W.; Yin, Y. D. *Angew. Chem., Int. Ed.* **2010**, *49*, 1862.

(4) (a) Shenhar, R.; Rotello, V. M. *Acc. Chem. Res.* **2003**, *36*, 549. (b) Lim, I. I. S.; Maye, M. M.; Luo, J.; Zhong, C. J. *J. Phys. Chem. B* **2005**, *109*, 2578.

(5) (a) Talapin, D. V.; Lee, J. S.; Kovalenko, M. V.; Shevchenko, E. V. *Chem. Rev.* **2010**, *110*, 389. (b) Chen, J.; Dong, A. G.; Cai, J.; Ye, X. C.; Kang, Y. J.; Kikkawa, J. M.; Murray, C. B. *Nano Lett.* **2010**, *10*, 5103. (c) Chen, Z. Y.; Moore, J.; Radtke, G.; Sirringhaus, H.; O'Brien, S. *J. Am. Chem. Soc.* **2007**, *129*, 15702. (d) Korgel, B. A. *Nat. Mater.* **2010**, *9*, 701. (e) Quan, Z.; Loc, W.; Lin, C.; Luo, Z.; Yang, K.; Wang, Y.; Wang, H.; Wang, Z.; Fang, J. *Nano Lett.* **2012**, *12*, 4409. (f) Choi, J.; Bian, K.; Baumgardner, W.; Smilgies, D.; Hanrath, T. *Nano Lett.* **2012**, *12*, 4791.

(6) Wulff, G. *Z. Krystallogr. Mineral.* **1901**, *34*, 449.

(7) *Handbook of Surface and Colloid Chemistry*; Birdi, K. S., Ed.; CRC Press: Boca Roton, FL, 1997.

(8) Klajn, R.; Bishop, K. J. M.; Grzybowski, B. A. *Proc. Natl. Acad. Sci. U.S.A.* **2007**, *104*, 10305.

(9) See the Supporting Information.

(10) Lum, K.; Chandler, D.; Weeks, J. D. *J. Phys. Chem. B* **1999**, *103*, 4570.

(11) Wu, H. M.; Chen, O.; Zhuang, J. Q.; Lynch, J.; LaMontagne, D.; Nagaoka, Y.; Cao, Y. C. *J. Am. Chem. Soc.* **2011**, *133*, 14327.

(12) Wang, Z. W.; Wen, X. D.; Hoffmann, R.; Son, J. S.; Li, R. P.; Fang, C. C.; Smilgies, D. M.; Hyeon, T. *Proc. Natl. Acad. Sci. U.S.A.* **2010**, *107*, 17119.

(13) Fuechsle, M.; Miwa, J. A.; Mahapatra, S.; Ryu, H.; Lee, S.; Warschkow, O.; Hollenberg, L. C. L.; Klimeck, G.; Simmons, M. Y. *Nat. Nanotechnol.* **2012**, *7*, 242.

(14) *Crystallization Technology Handbook*, 2nd ed.; Mersmann, A., Ed.; CRC Press: Boca Raton, FL, 2001.

(15) Lim, S. I.; Zhong, C. J. *Acc. Chem. Res.* **2009**, *42*, 798.

(16) (a) Kim, D. H.; Rozhkova, E. A.; Ulasov, I. V.; Bader, S. D.; Rajh, T.; Lesniak, M. S.; Novosad, V. *Nat. Mater.* **2010**, *9*, 165. (b) Hu, S. H.; Gao, X. H. *J. Am. Chem. Soc.* **2010**, *132*, 7234.

(17) Steketee, M. B.; Moysidis, S. N.; Jin, X.-L.; Weinsteini, J. E.; Pita-Thomas, W.; Raju, H. B.; Iqbal, S.; Goldberg, J. L. *Proc. Natl. Acad. Sci. U.S.A.* **2011**, *108*, 19042.